Land Management and Utilization
https://ojs.ukscip.com/index.php/lmu

ARTICLE

Influence of Shallow Water Table on Land Surface Temperature

Christian Alberto Mancino [1*] ***, Raúl Eduardo Rivas*** [1] ***, Raquel Niclòs*** [2]

[1] *Large Plains Hydrology Institute, Scientific Research Commission of the Province of Buenos Aires, Tandil 7000, Argentina*

[2] *Department of Earth Physics and Thermodynamics, Faculty of Physics, University of Valencia, Valencia 46100, Spain*

ABSTRACT

The influence of the Water Table (WT) and the capillary fringe plays a critical role in soil water dynamics, affecting plant-available water, soil moisture, evapotranspiration, and Land Surface Temperature (LST). This study examined the functioning of the aquifer–soil–plant–atmosphere system such as transpiration, evaporation, plant root water uptake and capillarity to assess how the WT and the capillary fringe affect LST. Field measurements were integrated with satellite data, including WT depth, precipitation records, and satellite-derived products such as LST, Normalized Difference Vegetation Index (NDVI), and potential evapotranspiration from reanalysis data (ERA5-Ag). The research was conducted in a shallow aquifer within the Salado River watershed, Buenos Aires Province, Argentina, over the period 2007–2023. Results revealed a strong inverse relationship (R^2 = 0.74) between the WT and LST. This relationship was modeled using an equation valid during the summer months, when atmospheric demand is high and soils are dry. The approach was validated using measurements from nearby piezometers, yielding a bias of −0.17 m and a root mean square deviation (RMSD) of 0.44 m. Satellite-derived LST was shown to effectively reflect the influence of the WT on plant transpiration under water-stressed conditions. By isolating the effect of evaporation, this method offers a novel means of indirectly assessing the hydrogeological status of shallow aquifers.

Keywords: Aquifer Shallow; Capillary Fringe; Vadose Zone; Soil Moisture; Transpiration; Piezometer; Landsat; Remote Sensing

*CORRESPONDING AUTHOR:
Christian Alberto Mancino, Large Plains Hydrology Institute, Scientific Research Commission of the Province of Buenos Aires, Tandil 7000, Argentina; Email: ch.a.mancino@gmail.com

ARTICLE INFO
Received: 28 June 2025 | Revised: 7 August 2025 | Accepted: 13 August 2025 | Published Online: 26 August 2025
DOI: https://doi.org/10.54963/lmu.v1i3.1550

CITATION
Mancino, C.A., Rivas, R.E., Niclòs, R., 2025. Influence of Shallow Water Table on Land Surface Temperature. Land Management and Utilization. 1(3): 1–15. DOI: https://doi.org/10.54963/lmu.v1i3.1550

1. Introduction

The WT and the capillary fringe are critical phenomena in soil water dynamics, directly affecting water availability for plants, evapotranspiration processes, and consequently, the land surface radiative temperature.

Both the WT and the capillary fringe are influenced by the relationship between atmospheric and hydraulic pressure. The upper limit of the capillary fringe is not sharply defined; rather, it constitutes a transitional zone where pore water content gradually decreases until reaching a region where pores are filled exclusively with air. This is particularly relevant for shallow aquifers under vegetation stress conditions, where deep roots cannot benefit from capillary rise. As a result, the system's LST increases in response to the limited availability of water for the transpiration process.

The depth of the WT varies depending on factors such as topography, precipitation, and soil characteristics, while the capillary fringe may extend from just a few centimeters in sandy soils to several meters in clayey soils due to differences in pore size [1,2].

When the WT is near the surface, the capillary fringe may reach the root zone, providing an additional water source, especially during periods of agricultural drought. Root depth and water extraction capacity are adapted to local soil conditions and water availability [3,4], thus enabling plants to access water from the capillary fringe. In scenarios with a shallow WT, roots tend to develop closer to the surface and draw water directly from the capillary fringe. This becomes particularly important in soils with high water retention capacity, such as clay-loam soils found in low-slope areas with a humid temperate climate. Therefore, in the absence of precipitation inputs and under sustained evapotranspiration, soil moisture decreases, leading to a drop in the WT.

In a conceptual model where no precipitation enters the system (i.e., the vadose zone is dry), evaporation approaches zero. Under these conditions, the capillary fringe plays a key role by supplying water to plant roots. In the context of the water deficit, a shallow WT and a well-developed capillary fringe promote transpiration and significant leaf development, reflected in high NDVI values. Transpiration cools the land surface through the release of water vapor, which absorbs heat during the process (resulting in high NDVI values), thereby reducing land surface temperature (**Figure 1a**). In contrast, a deeper WT and a limited capillary fringe may reduce water availability for transpiration, leading to diminished leaf development (a decline in NDVI) and resulting in an increase in surface temperature (**Figure 1b**). The relationships among the WT, the capillary fringe, plant roots, and transpiration have significant effects on LST.

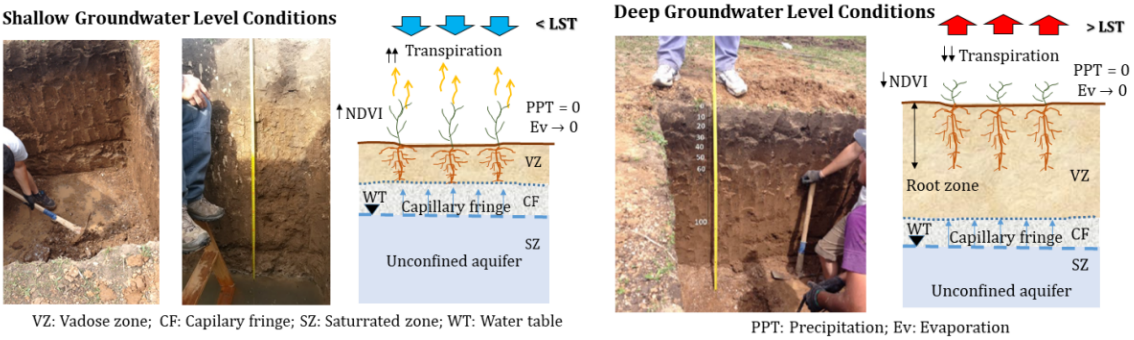

Figure 1. Conceptual model of system functioning in the study area. (**a**) Shallow WT; (**b**) Deep WT.

The conceptual model shown in **Figure 1a** and **Figure 1b** highlights that the interaction between the WT, the capillary fringe, LST, and transpiration is essential for understanding land surface processes and dynamics. These processes account for geological, geomorphological, climatic, and biological factors that influence groundwater behavior, typical of flatland regions such as the Salado River watershed in the Pampean region of Argentina [5,6].

The WT and soil texture directly influence the de-

velopment of the capillary fringe, which in turn determines the depth and distribution of the plant root system. This relationship regulates the energy availability within the system, controlling both the magnitude of transpiration and heat transfer processes.

This study focuses on understanding the functioning of the aquifer–soil–plant–atmosphere system in a sector of the Pampas region, Buenos Aires Province, Argentina, using both in situ data and satellite-derived information. The hypothesis is that LST may respond to the influence of WT dynamics. This is assessed through the analysis of in situ observations (WT and precipitation) and satellite and reanalysis derived products including (LST, Hargreaves potential evapotranspiration (ETp), potential water deficit (PPT–ETo), and NDVI) over the period from February 2007 to December 2023.

2. Background

Several studies have explored the relationship between soil moisture, the WT, and LST, considering diverse geographic settings and methodologies. In this context, Kappelmeyer [7] conducted in situ soil temperature measurements at a depth of 1.5 m to detect fractures carrying warm water, although the study did not specify the location, duration, soil type, or vegetation.

In contrast, Chase [8] carried out research in southern Alberta, Canada, on glacial sediment soils and salt flats covered by grasslands, using airborne remote sensing to measure radiative temperatures over large areas. Subsequently, Myers and Moore [9] performed a one-day summer study in the Midwestern United States, using airborne thermal radiometers to correlate surface temperature with aquifer thickness in glacial sediments.

With the advent of remote sensing, it became possible to measure radiative temperatures over extensive areas. Accordingly, Heilman and Moore [10] conducted a study in South Dakota (USA) on tilled glacial deposit soils planted with oats, wheat, barley, and corn. They used both in situ measurements and data from the Heat Capacity Mapping Mission (HCMM) to relate daytime land surface temperature to WT depth.

More recently, Alkhaier et al. [11] conducted a yearlong study on loam-textured soils without vegetation, under a climate characterized by hot, dry summers and cool, humid winters. They employed numerical simulations and in situ measurements of both shallow and deep WT to assess how shallow groundwater influences land temperature and surface energy balance.

Similarly, Pablos et al. [12] investigated soil moisture dynamics and LST over daily and seasonal timescales in the Duero River Watershed (Spain) over a four-year period. Although the study did not specify soil or vegetation types, it combined in situ measurements with satellite data from the Moderate Resolution Imaging Spectroradiometer (MODIS) mission.

In a comparable line of research, Hamzeh et al. [13] examined the relationship between WT and LST in southwestern Iran on saline, unvegetated soils, using Landsat 8 imagery. Finally, Subzar Malik et al. [14] analyzed the effect of WT on soil moisture, surface temperature, and LST in alluvial agricultural soils during the six months preceding the monsoon season in the Tawa River Watershed (India), using both in situ data and Landsat 8 images.

Collectively, these studies highlight a range of methodologies covering different seasonal periods, climates, WT depths, soil types, vegetation covers, and satellite sensors. However, none of them focus specifically on the integrated functioning of the system as addressed in this study.

3. Materials and Methods

The processing and analysis chain for field data, satellite products, and reanalysis datasets was conducted using MATLAB, QGIS, and Excel spreadsheets, following the workflow outlined in **Figure 2**.

3.1. Field Data

3.1.1. Water Table Measured from Piezometer P10

The WT data were measured from piezometer P10 (La Madrugada ranch), located in the sub-watershed of Del Azul stream on the southern slope of the Salado River (latitude: −36° 22.6′; longitude: −59° 29.3′; elevation: 69.9 m a.s.l.), Buenos Aires Province, Argentina (**Figure**

3a and Figure 3b). This piezometer is part of a monitoring network of 35 wells established by the Large Plains Hydrology Institute[15] (https://ihlla.conicet.gov.ar), and data can be accessed in the network's database (http://www.azul.bdh.org.ar). The WT data were recorded discontinuously for the 2007–2023 time series. Automatic, instantaneous measurements (one reading per hour) are available from February 2007 to October 2010, and from May 2017 to December 2022. Manual measurements (one reading every 15 days) were taken from June 2011 to June 2016 and from May 2023 to December 2023. The data collection equipment consisted of a GENICA LF 324 water level logger (with an accuracy of ±5 mm) for instantaneous records and a level probe (±5 mm measurement error) for biweekly measurements. The lithological description of the borehole where the piezometer was installed is provided in **Appendix A, Figure A1**.

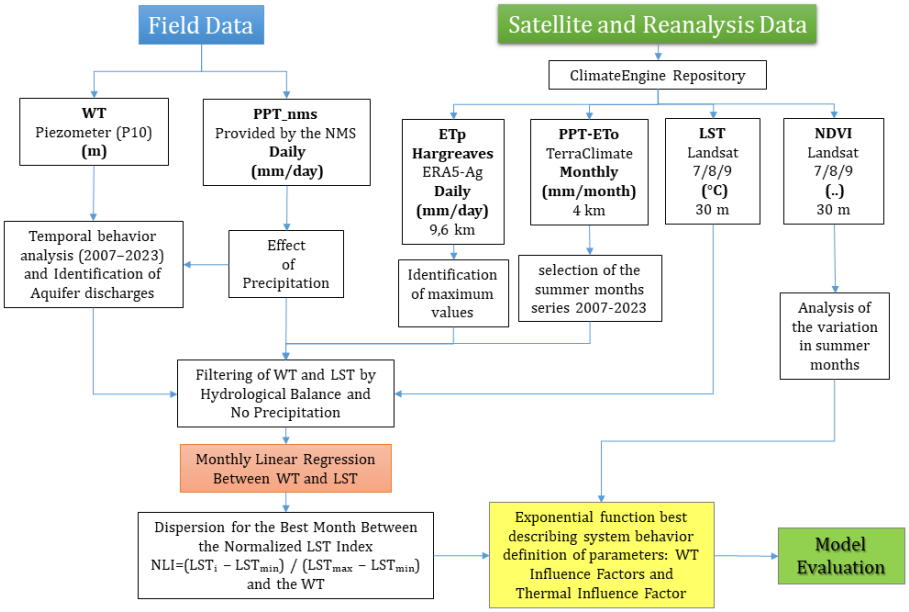

Figure 2. Workflow diagram with different temporal resolutions: daily and monthly scales.

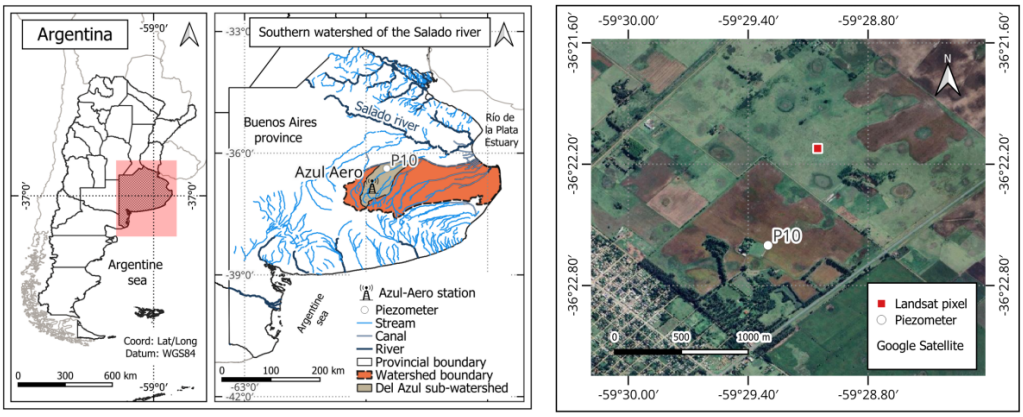

(**a**) (**b**)

Figure 3. (**a**) Location of the study area highlighting the watershed of the southern slope of the Salado River (Orange area, 40000 km^2) and the sub-watershed of Del Azul Stream (Gray area, 6200 km^2). The meteorological station Azul-Aero and the piezometer used (P10) are located within Del Azul Stream sub-watershed; (**b**) Detail of the location of the piezometer P10 on a true-color composite Google Satellite image. The central point (red square) indicates the reference pixel location used for the analysis with satellite-derived data.

3.1.2. Precipitation from Argentine National Meteorological

Precipitation data were obtained from the online repository of the National Meteorological Service of Argentina (https://www.smn.gob.ar). The precipitation values obtained from this repository (PPT_nms) cover the 2007–2023 period and are provided as daily records in mm/day. The closest weather station is located in the city of Azul (referred to as Azul-Aero), approximately 55 km from the location of the piezometer.

Considering the effect of precipitation is essential when analyzing the influence of the WT and the capillary fringe on LST. Heavy rainfall can saturate the soil, masking the contribution of the capillary fringe to the transpiration process. Therefore, an exclusion criterion was applied: all records with rainfall during the two days prior to the satellite overpass were removed. The other two exclusion criteria applied are described in Sections 3.2.1 and 3.2.3.

Once the WT and precipitation data were compiled and reorganized, a temporal analysis was conducted to identify groundwater recharge and discharge periods, based on sustained rises or declines in the WT and corresponding precipitation trends.

3.2. Satellite and Reanalysis Data

Satellite-derived products were obtained from the ClimateEngine.org repository (www.climateengine.org). The selected pixel (30 m × 30 m) for data extraction is located approximately 950 m northeast of the piezometer (**Figure 3b**). Since the piezometer is located within a parcel cultivated with seasonal pasture, a nearby area dominated by natural grasslands used for cattle grazing was selected. The difference in WT depth due to this spatial shift is considered negligible, as the terrain slope is approximately 0.05º. Therefore, the measurements can be regarded as representative for the analysis.

3.2.1. Hargreaves ETp Product

The ETp uses a simplified approach that requires only temperature and incoming radiation data [16]. This model can be applied to estimate ETp using a wide range of datasets, including the global ERA5 and ERA5-Ag reanalysis datasets. The latter is a daily surface meteorological dataset specifically designed for agricultural and agroecological studies, covering the period from 1979 to the present. It is based on the hourly ERA5 reanalysis data from the European Centre for Medium-Range Weather Forecasts (ECMWF), with ERA5-Ag providing post-processed and aggregated data for direct use in agricultural applications. The data are adjusted to a higher-resolution topography, offering a spatial resolution of approximately 9.6 km and a daily temporal resolution (mm/day). Detailed information and data access are available through the Copernicus Climate Change Service [17].

This product was used to identify peak soil water demand (daily/monthly) and to compute the water balance between PPT_nms and ETp. These metrics complement the analysis presented in Section 3.1.2, as they help to isolate days and months of the year during which precipitation does not interfere with the influence of the capillary fringe on plant transpiration.

The choice of the Hargreaves method is based on its simplicity, the low data requirements (only temperature and radiation), and the high compatibility with reanalysis datasets such as ERA5-Ag. The latter provides daily data with a spatial resolution of 9.6 km, enabling the analysis of daily temporal patterns that ensure the applicability of the proposed conceptual model.

3.2.2. LST Product

The LST product from ClimateEngine.org is an operational Level 2 product derived from Landsat 7/8/9 satellites through a multi-step process involving data acquisition, atmospheric correction, surface emissivity estimation, and final LST calculation, as follows:

- Thermal data acquisition: Thermal measurements are obtained from the thermal bands of the ETM+ sensor (Landsat 7) and TIRS sensors (Landsat 8/9). These thermal bands provide the radiance values required to compute LST.
- Radiometric correction: The digital numbers are converted to radiance values through radiometric calibration of the imagery.
- Atmospheric correction: This step is based on atmospheric profiles obtained from reanalysis models, including the National Centers for Environmen-

tal Prediction (NCEP) and NASA's Modern-Era Retrospective analysis for Research and Applications (MERRA).

- Surface emissivity estimation: Surface emissivity is estimated using global emissivity datasets, particularly the ASTER Global Emissivity Database (GED).
- LST calculation: A Single-Channel Algorithm based on the radiative transfer equation is applied to convert thermal radiance into brightness temperatures. These are then corrected for emissivity and atmospheric effects using atmospheric profile-derived parameters to retrieve LST.

The spatial resolution of the final LST product is 30 meters (resampled from the original thermal bands of 60 and 100 meters), and the temporal resolution is instantaneous, based on satellite overpass (every 8 days, when combining multiple Landsat missions), specifically at 10:10 a.m. LST is reported in degrees Celsius (°C).

A more detailed description of the methodology used for this product can be found in Malakar et al.[18] and Li et al.[19]. Additionally, Niclòs et al.[20] provide validation of the Landsat 9 TIRS-derived LST product over vegetated areas, showing an accuracy of approximately 1 K.

3.2.3. PPT–ETo Product (Potential Water Deficit)

The potential water deficit is an index that relates precipitation (PPT) and reference evapotranspiration (ETo, mm/month). When the value is negative, it indicates that precipitation is insufficient to sustain the evapotranspiration process, which may signal potential drought or water stress for vegetation.

To support a more robust analysis of the LST, this product was used to identify the months within the time series that exhibit the highest water deficit. In humid and sub-humid regions such as the study area, summer is typically the period with the highest water demand, during which evapotranspiration exceeds precipitation, and the most significant water deficits are observed. Accordingly, analyses were focused on these periods—when the soil is drying out and no water is stored within the root zone of the soil profile—thus eliminating the "noise" generated by precipitation in the vadose zone.

This represents the final exclusion criterion, as referenced in section 3.1.2. Therefore, water input to the analyzed system can be attributed solely to upward flow from the WT and the capillary fringe.

3.2.4. NDVI Product

A common satellite-derived index used to assess vegetation vigor is the Normalized Difference Vegetation Index (NDVI)[21,22], which ranges from −1 to 1, with values 0.5 to 1 indicating high vegetation vigor.

NDVI data were used to assess vegetation dynamics over the analyzed time series, following the approach proposed by Holzman et al.[23], who linked NDVI and satellite derived LST with the evapotranspiration process. Within this conceptual framework, a bare soil surface characterized by low NDVI and high LST indicates conditions where evaporation is nearly absent. Conversely, a surface with low LST and high NDVI values represents active vegetation cover, associated with transpiration occurring near its maximum potential.

In this study, NDVI was derived from Landsat 7/8/9 imagery, based on the difference in reflectance between the red (visible) and near-infrared (NIR) spectral bands. The spatial resolution is 30 m, and the temporal resolution corresponds to the satellite overpasses (ranging from 1 to 16 days).

3.3. Normalized Land Surface Temperature Index (NLI)

A Normalized Land Surface Temperature Index (NLI) was applied as an indicator of water availability for the evapotranspiration process, as shown in Equation 1:

$$\mathrm{NLI} = (\mathrm{LSTi} - \mathrm{LSTmin})/(\mathrm{LSTmax} - \mathrm{LSTmin}) \quad (1)$$

Where:

- $\mathrm{LST_i}$ is the land surface temperature corresponding to the pixel at the time of satellite overpass;
- LSTmax is the maximum land surface temperature recorded for that pixel across the multi-year time series;
- LSTmin is the minimum land surface temperature recorded for that pixel across the same time series.

NLI values range from 0 to 1, where:

- Values near 0 indicate thermally favorable conditions for evapotranspiration, i.e., relatively low pixel temperatures;
- Values near 1 indicate thermally extreme conditions, with temperatures approaching the historical maximum for the pixel, which implies limitations for evapotranspiration.

4. Results

In the southern flank of the Salado River, evapotranspiration processes greatly exceed those of infiltration and runoff, resulting in WT fluctuations associated with aquifer recharge and discharge periods. Discharge periods are particularly relevant for this study and vary according to the hydrogeological cycle considered, depending on antecedent precipitation and soil moisture within the vadose zone. Within this context, and following the established methodological framework, the results are presented. **Table 1** shows basic statistics for the 2007–2023 time series of the analyzed variables.

The values presented in **Table 1** show that when the WT reaches its minimum depth, close to 0.58 m, there are no apparent limitations on the occurrence of the evapotranspiration process. In this case, the NLI tends toward values near 0, indicating that the temperature of the pixel associated with the area where the piezometer is located approaches the LSTmin. Conversely, when the WT reaches values near the maximum depth of 5.36 m, the connection between the aquifer and the atmosphere weakens or is interrupted, resulting in the suppression of the evapotranspiration process. Under these conditions, the NLI tends toward 1, and the corresponding pixel shows temperatures near the LSTmax. This situation can be interpreted as a functional disconnection between the subsurface system and the depth of the vegetation roots.

Table 1. Descriptive statistics of the analyzed variables for the entire 2007–2023 time series: LST, WT, PPT_nms, and ETp using the Hargreaves method.

Statistic	Smoothed LST [°C]	WT [m]	PPT_nms [mm/day]	ETp [mm/day]
Maximum	44.4	5.36	173.5	7.8
Minimum	7.0	0.58	0.0	0.5
Average	24.1	2.90	2.5	3.2

During the analyzed period, eight hydrogeological cycles were identified. Each hydrological cycle is composed of discharge and recharge periods (**Figure 4**). Discharge periods are characterized by prolonged declines in the WT caused by annual precipitation below the average and a high water deficit (PPT–ETo). Recharge periods are characterized by a rise in the WT due to high precipitation and elevated soil moisture in the vadose zone. This distinction is clearly observed in Cycle 1, when from 2008 to 2011, precipitation remained below average, leading to a decline in WT from 2.34 m to 5.63 m (the maximum decline observed in the study period). Then, in 2012, precipitation nearly doubled the average, resulting in a rise of the WT to 1.38 m.

Identifying the discharge periods is essential for this study, as they represent the moments when the contribution of precipitation to the aquifer is minimal. The maximum daily values of Hargreaves ETp (mm/day), derived from ERA5-Ag reanalysis data, occur in January and correspond to the peaks of soil water consumption. The daily water deficit, calculated as the difference between PPT_nms and Hargreaves ETp for precipitation-free days, ranges between −4.1 and −6.8 mm/day in January. Daily statistics for the month of January are presented in **Appendix A, Table A1**.

Figure 5 presents an analysis of satellite imagery captured by the MODIS sensor (RGB143 bands), identifying two distinct aquifer states. January 2010 followed more than three consecutive years of below-average precipitation (blue dashed line), which led to a WT decline to 4.7 m (**Figure 4**) and resulted in a hydrological deficit. In contrast, September 2014 was preceded by 18 months of above-average WT levels (orange dashed line), along with abundant rainfall during that year. This combination caused the WT to rise to approximately 0.7 m below the surface (**Figure 4**), resulting in flooding in the lower

watershed. The hydrological deficit condition is evident in **Figure 5a**, while excess water is indicated by the black-colored areas in **Figure 5b**.

Figure 6 shows the monthly relationship between the WT and LST for the 2007–2023 period. The correlations are positive in most months, except for February and March, where they are negative. January showed the strongest correlation, with an R^2 of 0.74, indicating that there is no influence from surface water inputs during this period, and that the variation in LST is explained by the WT depth. Therefore, January was selected for the detailed analysis. This choice also aligns with the seasonal period analyzed by Myers and Moore [9], Heilman and Moore [10], Hamzeh et al. [13] and Subzar Malik et al. [15].

The values of the monthly potential water deficit (PPT–ETo) were used to identify the January months with the highest water deficit, ensuring that the capillary effect can be observed. **Table 2** shows the difference between monthly precipitation and reference evapotranspiration (PPT–ETo) for January during the analysis period. The years 2011 and 2019 were excluded from the analysis due to excess water, which may have influenced surface temperature due to increased soil moisture in the vadose zone.

The vegetation status for the selected January months shows NDVI values ranging from a minimum of 0.27 to a maximum of 0.74, while LST values range from a maximum of 44.4 °C to a minimum of 30.5 °C.

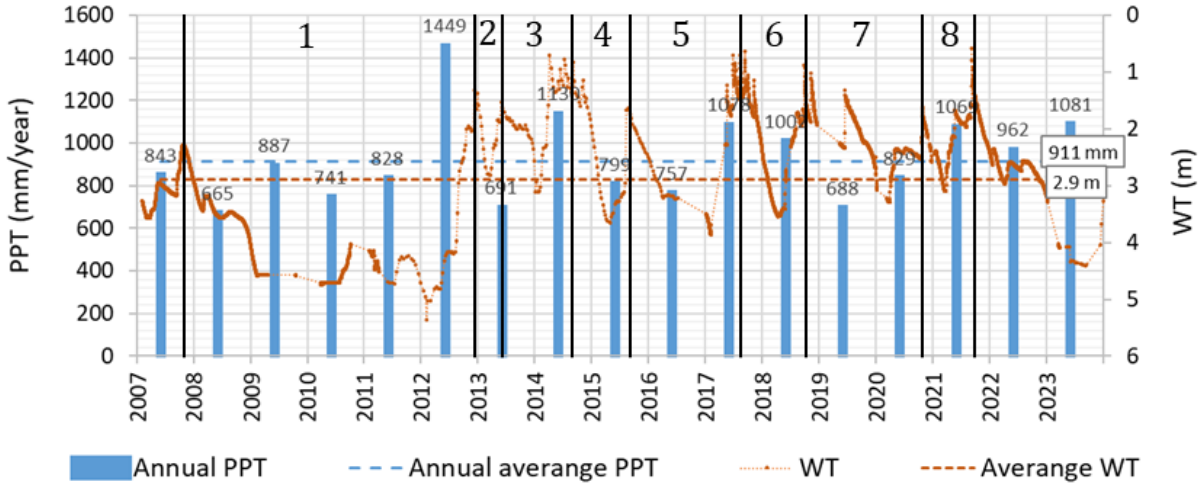

Figure 4. Fluctuations of the daily WT data together with annual PPT_nms. Eight hydrogeological cycles are identified between solid black lines, each comprising recharge and discharge periods of the aquifer for the 2007–2023 series. The horizontal dashed lines represent the annual averages of PPT_nms and WT data.

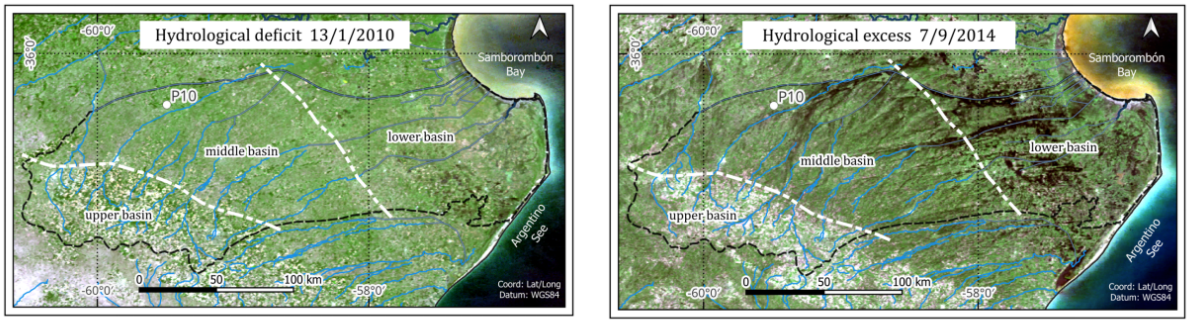

(**a**) (**b**)

Figure 5. Influence of the WT under two different hydrological conditions, shown over a true-color composite image (RGB143) from sensor MODIS instrument aboard EOS-Aqua/Terra satellites. White dashed lines indicate the boundaries of the upper, middle, and lower watersheds. (**a**) Drought in January 2010, with limited surface water and deep WT levels due to hydrological deficit; (**b**) Flooding in September 2014 with shallow WT levels, where black tones in the image indicate very wet soils or surface water.

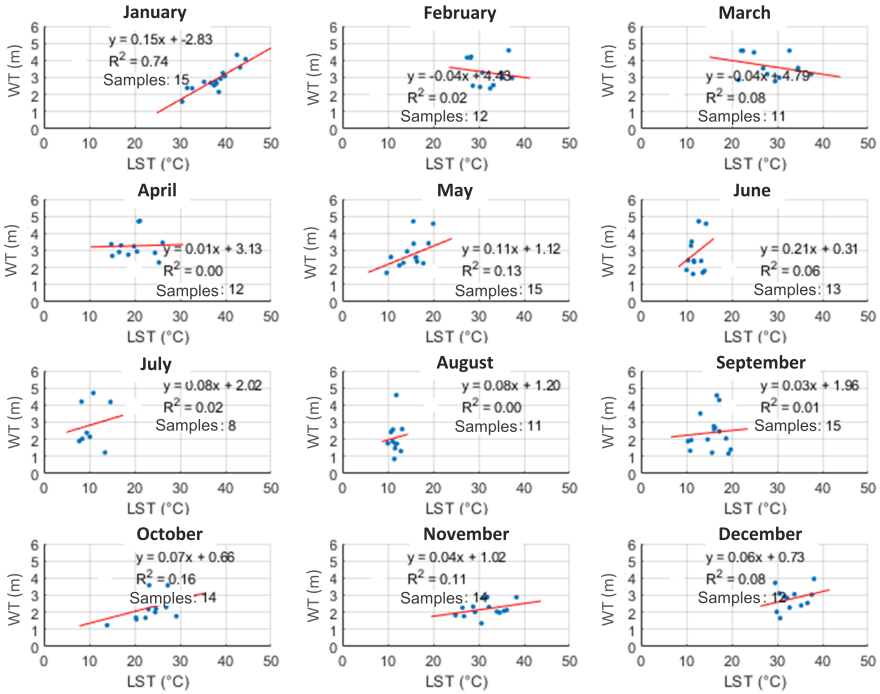

Figure 6. Linear regressions of daily WT levels versus daily LST for the period 2007–2023. The dataset was filtered to remove the effects of precipitation.

Table 2. Water availability (PPT–ETo) for the month of January.

Year	Month	PPT–ETo [mm]
2008	Jan	−64.4
2009	Jan	−177.3
2010	Jan	−92.4
2011	Jan	+2.7
2012	Jan	−119.0
2013	Jan	−136.0
2014	Jan	−13.6
2015	Jan	−60.1
2016	Jan	−56.6
2017	Jan	−83.4
2018	Jan	−94.4
2019	Jan	+11.7
2020	Jan	−124.6
2021	Jan	−64.8
2022	Jan	−17.0
2023	Jan	−113.9

A scatterplot was generated between WT and NLI in order to fit a function that describes the behavior of the aquifer–atmosphere system, resulting in Equation 2:

$$WT = \alpha \cdot e^{\beta \cdot NLI} \quad (1)$$

Where:

- α is the WT influence factor coefficient (meters)
- e is the exponential function
- β is the thermal influence factor coefficient (dimensionless).
- NLI is the Normalized Land Surface Temperature Index (dimensionless), defined in Equation 1.

Equation 2 indicates that when the NLI approaches zero, the WT depth is at its minimum, implying maximum influence of the aquifer on the plant transpiration process. Under these conditions, the LSTi tends to converge toward the LSTmin value. An exponential function was selected for the fit based on the characteristic

behavior of groundwater level declines, which often follow an exponential trend due to the nature of water flow in aquifers and the hydraulic properties of the porous medium. As the WT declines, the hydraulic pressure gradient decreases over time and with distance from the discharge point, resulting in a flow pattern that can be described by exponential functions.

Figure 7 illustrates the interpretation of this correlation. When the NLI approaches zero, the curve intersects the shallowest WT level attainable by the aquifer that still ensures water supply for plant transpiration. Under these conditions, plant roots are able to extract water directly from the capillary fringe, promoting maximum foliage development (indicated by NDVI values approaching their upper limit). As water vapor is released during transpiration, latent heat is absorbed from the system, cooling the land surface, and reducing the LSTi. Therefore, the influence of the WT on the plant is at its highest (**Figure 7**). Conversely, when the temperature ratio approaches one, the influence of the WT on root water uptake becomes negligible. As a result, transpiration decreases, which is reflected by an increase in LST. This interpretation aligns with the conceptual model described in **Figure 1**.

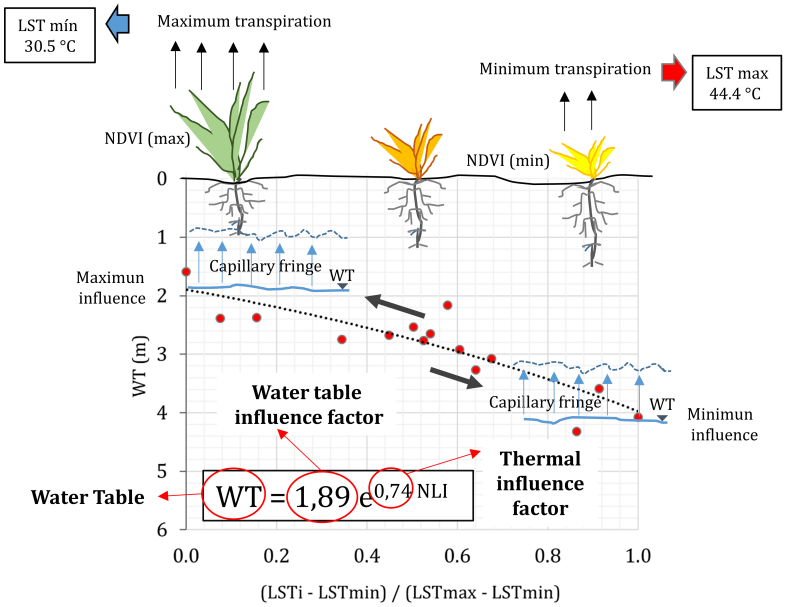

Figure 7. Behavior of the WT Influence Factor on transpiration, NDVI, and LST.

5. Model Evaluation

To evaluate the fitted exponential function, data from piezometers belonging to the monitoring network of the Large Plains Hydrology Institute in the Del Azul sub-watershed (southern slope of the Salado River), Buenos Aires Province, were used. The analysis included seven piezometers located in the middle-lower sub-watershed, with in situ WT measurements corresponding to January 2018. This year was selected because the recorded precipitation was minimal and no aquifer recharge was observed, resulting in a significant hydrological deficit (-94.4 mm). This ensures the applicability of the proposed model under conditions of limited recharge.

Comparisons were made between observed and modeled WT values by applying the developed exponential function. The lithological description of the boreholes where the piezometers were installed is similar [15]. Therefore, the comparison is considered valid based on the available knowledge in the database (http://www.azul.bdh.org.ar), which shows that fluctuations in the unconfined aquifer's WT exhibit spatially consistent behavior and representativeness.

The data used and the associated statistics are presented in **Table 3** and **Table 4**. The most significant differences were observed at piezometers P20 and P06, likely due to variations in the subsurface lithological pro-

file compared to the lithology on which the model was developed. Soil profiles with higher clay content induce greater capillary rise compared to silty-sandy soils. Additionally, the presence of calcrete layers may act as a sealing barrier, limiting the upward movement of the WT table and partially confining the aquifer. However, this does not mean that plant roots cannot penetrate these calcrete layers. In the remaining piezometers, the discrepancies between observed and modeled WT levels were minimal.

Table 3. Measured and estimated WT values, and differences for model validation.

Piezometer	Modeled WT [m]	Measured WT [m]	Modeled–Measured WT [m]
P03	2.18	1.87	+0.31
P05	2.37	2.24	+0.13
P06	1.92	2.47	−0.55
P07	2.07	1.61	+0.46
P08	2.16	2.36	−0.20
P09	2.53	2.16	+0.37
P20	2.67	2.03	+0.64

Table 4. Standard deviation (SD) of the differences, root-mean-square difference (RMSD; the quadratic sum of bias and SD).

BIAS [m]	SD [m]	RMSD [m]
0.17	0.41	0.44

Figure 8a shows the NDVI distribution map, with most values ranging between 0.50 and 0.70, indicating significant leaf development associated with plant transpiration processes. **Figure 8b** displays the modeled WT influence in the lower sub-watershed of the Azul stream, along with the differences observed at each piezometer used in the evaluation. A homogeneous WT distribution is observed across the central-southern and western sectors, with increasing depth toward the northwest.

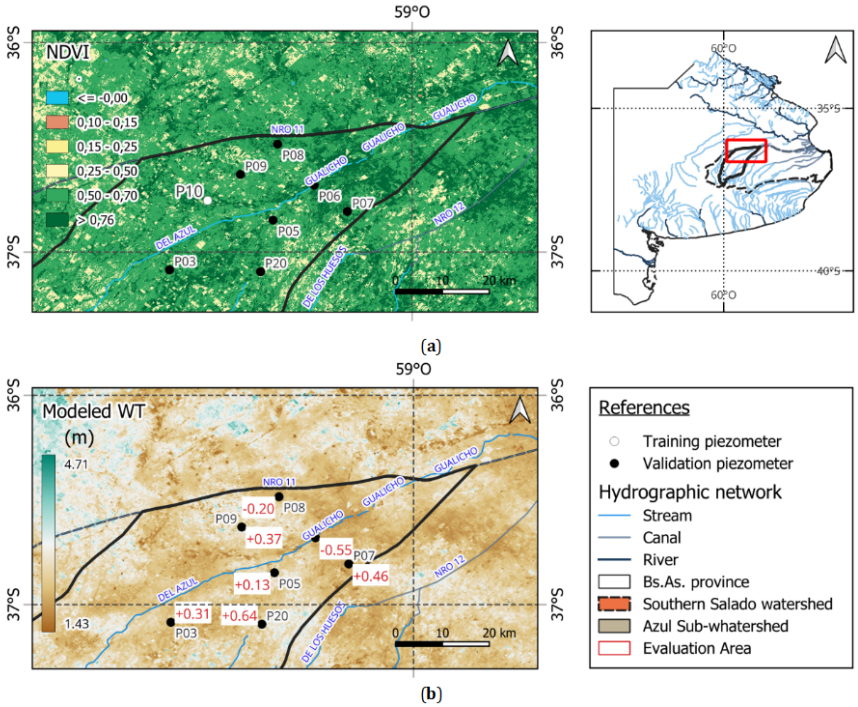

Figure 8. (**a**) NDVI map over the lower Azul sub-w watershed in the model evaluation area; (**b**) Map showing the influence of the modeled WT and the locations of the piezometers used for validation. The numbers in white rectangles indicate the differences between measured and modeled values. The maps correspond to January 28, 2018, and were generated using Landsat 8 imagery with a spatial resolution of 30 meters.

6. Conclusions

This study presents a detailed analysis of a shallow aquifer and its interaction with the soil–plant–atmosphere system, proposing a model capable of evaluating the effect of the WT on plant transpiration. To this end, WT data from the Pampeano Aquifer located in the Azul Creek sub-watershed (southern slope of the Salado River) were integrated with satellite observations and reanalysis products.

The main findings indicate that LST derived from satellite data can reveal how WT dynamics and the capillary fringe affect plant transpiration, as reflected in the thermal behavior of the land surface. Results show that the connection between the aquifer and the atmosphere follows an exponential function, whose validity depends on the near-minimum moisture content in the vadose zone. Under these conditions, LST becomes a reliable proxy for subsurface conditions.

To characterize the aquifer using LST, the parameters of an exponential function—defined by the WT influence factor and a thermal factor—must be estimated under the following conditions:

1. There must be no water input from precipitation, ensuring the aquifer is in a discharge state.
2. The daily water balance must be negative, indicating no water availability in the vadose zone for plant transpiration (soil evaporation under such conditions should be negligible).
3. The monthly water balance must also be significantly negative.

When these conditions are met, it is possible to estimate the upper and lower bounds of WT influence using LST data obtained from satellite imagery.

The scatterplot between WT and the NLI based on 16 years of data allowed for the definition of the WT influence factor (α) and the thermal factor (β) included in Equation 2, with α = 1.89 m and β = 0.74. Once these parameters were determined, the model was validated using in situ WT measurements from seven piezometers recorded in January 2018, yielding a BIAS of 0.17 m and a root-mean-square difference (RMSD) of 0.44 m. These values indicate that the method performs well as an indirect estimator of the aquifer's hydrogeological conditions.

This work represents an advancement over previous studies that employed LST as an indicator under different hydro-environmental conditions. Unlike earlier approaches, this method excludes the effect of soil evaporation from the system analysis, allowing for the development of a more robust model based on an exponential function that more accurately captures WT declines and their influence on aquifer dynamics, vegetation, and LST.

The practical implications of this study are relevant for water resource management in agricultural and pastoral regions lacking extensive in situ monitoring. The methods developed here may be applied to other aquifers, provided the established conditions are met. In a context of increasing climate variability and more frequent extreme events, this methodology offers a valuable tool for monitoring shallow aquifers.

Finally, it is concluded that, given a sufficiently long time series of WT measurements, satellite data, and products derived from the integration of satellite and reanalysis information, the proposed method can be replicated in other regions with similar environmental settings.

Author Contributions

Conceptualization, C.A.M. and R.E.R; methodology, C.A.M, R.E.R and R.N.; software, C.A.M.; validation, C.A.M and R.E.R.; formal analysis, C.A.M. and R.E.R.; investigation, C.A.M, R.E.R and R.N.; resources, C.A.M.; data curation, C.A.M, R.E.R and R.N.; writing—original draft preparation, C.A.M.; writing—review and editing, C.A.M, R.E.R and R.N.; visualization, C.A.M.; supervision, R.E.R and R.N.X.X.; project administration, C.A.M.; funding acquisition, C.A.M. All authors have read and agreed to the published version of the manuscript.

Funding

This work was supported by public funds from the Province of Buenos Aires, Argentina.

Institutional Review Board Statement

Not applicable.

Informed Consent Statement

Not applicable.

Data Availability Statement

The data supporting the results can be found on the following websites: Hydrological database of the Azul stream basin (http://www.azul.bdh.org.ar/), repository of the National Meteorological Service of Argentina (https://www.smn.gob.ar/), and the repository of climatic, hydrological, and remote sensing data Climate Engine (www.climateengine.org).

Acknowledgments

The first author acknowledges the Large Plains Hydrology Institute and the Scientific Research Commission of the Province of Buenos Aires (both publicly funded institutions) for supporting his training in Remote Sensing.

Conflicts of Interest

The authors declare no conflicts of interest.

Appendix A

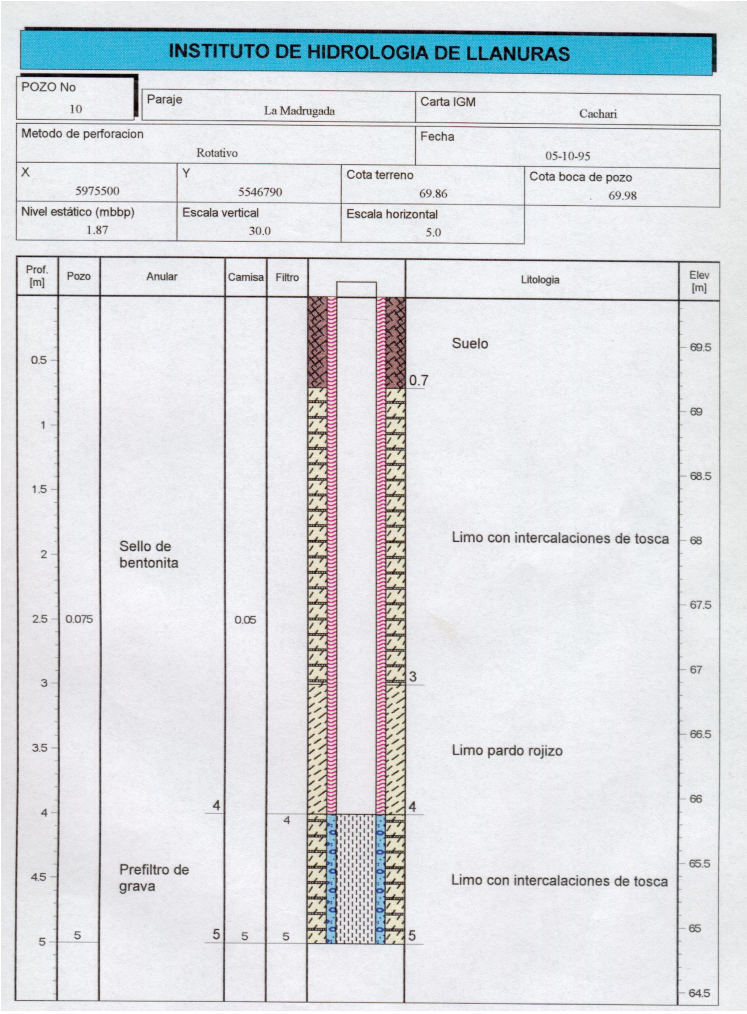

Figure A1. Lithological description of the borehole where piezometer P10 is installed.

Table A1. Descriptive statistics of the analyzed variables for the month of January.

Date	Original LST [°C]	Smoothed LST [°C]	(LSTi-LSTmin)/ (LSTmax-LSTmin) [...]	WT [mm]	ETp [mm]	PPT_nms-ETp [mm]	NDVI [...]
2008/01/17	40.62	39.89	0.68	3.08	5.34	−5.34	0.44
2009/01/03	43.69	44.41	1.00	4.08	6.27	−6.27	0.33
2009/01/19	41.34	42.51	0.86	4.32	6.01	−6.01	0.32
2013/01/06	31.56	30.49	0.00	1.59	6.47	−6.47	0.74
2014/01/17	44.92	38.91	0.60	2.92	6.61	−6.61	0.48
2015/01/12	40.96	38.53	0.58	2.16	6.66	−6.66	0.35
2016/01/07	39.13	37.49	0.50	2.54	6.00	−6.00	0.33
2016/01/23	36.45	38.01	0.54	2.65	4.57	−4.57	0.31
2016/01/31	34.11	35.28	0.34	2.75	4.50	−4.50	0.27
2017/01/17	44.80	43.21	0.91	3.59	6.80	−6.80	0.38
2018/01/20	39.53	36.73	0.45	2.68	6.10	−6.10	0.27
2018/01/28	36.06	37.80	0.52	2.77	5.75	−5.75	0.34
2021/01/20	35.87	31.53	0.07	2.39	6.28	−6.28	0.64
2022/01/31	30.30	32.66	0.16	2.37	4.14	−4.14	0.61
2023/01/10	46.03	39.40	0.64	3.27	6.48	−6.48	0.50
Maximum	46.03	44.41	0.00	4,32	6.80	−4.14	0.74
Minimum	30.30	30.49	1.00	1.59	4.14	−6.80	0.27
Average	39.02	37.79	0.52	2.88	5.86	−5.86	0.42

References

[1] Lexow, C., Bonorino, A.G., 2003. Definition of the Capillary Fringe in a Shallow Loessic Phreatic Aquifer. Proceedings of the III Argentine Congress of Hydrogeology and I Hispano-Latin American Seminar on Current Issues in Groundwater Hydrology. (1), 179–187. (in Spanish)

[2] Dingman, S.L., 2002. Physical Hydrology. Prentice-Hall Inc.: Upper Saddle River, NJ, USA.

[3] Sakalauskas, K.M., Costa, J.L., Laterra, P., et al., 2001. Effects of burning on soil-water content and water use in a Paspalum quadrifarium grassland. Agricultural Water Management. 50(2), 97–108. DOI: https://doi.org/10.1016/S0378-3774(01)00095-6

[4] Nosetto, M.D., Jobbágy, E.G., Brizuela, A.B., et al., 2012. The hydrologic consequences of land cover change in central Argentina. Agriculture, Ecosystems & Environment. 154, 2–11. DOI: https://doi.org/10.1016/j.agee.2011.01.008

[5] Kruse, E., Zimmermann, E., 2002. Hydrogeology of Large Plains: Particularities in the Pampean Plain (Argentina). In Proceedings of the XXXII IAH Congress: Groundwater and Human Development, Mar del Plata, Argentina; pp. 2025–2038. (in Spanish)

[6] Auge, M.P., 2022. Hydrogeological Environments of the Province of Buenos Aires, Argentine Republic. In Proceedings of the XI Argentine Congress of Hydrogeology, Bahía Blanca, Argentina, 25–28 October 2022; Available from: http://sedici.unlp.edu.ar/handle/10915/154035 (cited 20 August2025). (in Spanish)

[7] Kappelmeyer, O., 1957. The use of near surface temperature measurements for discovering anomalies due to causes at depths. Geophysical Prospecting. 5, 239–258.

[8] Chase, M.E., 1969. Airborne remote sensing for groundwater studies in prairie environment. Canadian Journal of Earth Sciences. 6, 737–741.

[9] Myers, V.I., Moore, D.G., 1972. Remote sensing for defining aquifers in glacial drift. In Proceedings of the Eighth International Symposium on Remote Sensing of Environment, University of Michigan, Ann Arbor, MI, USA; pp. 715–728.

[10] Heilman, J.L., Moore, D.G., 1982. Evaluating depth to shallow groundwater using heat capacity mapping mission (HCMM) data. Photogrammetric Engineering and Remote Sensing. 48, 1903–1906.

[11] Alkhaier, F., Flerchinger, G.N., Su, Z., 2012. Shallow groundwater effect on land surface temperature and surface energy balance under bare soil conditions: modeling and description. Hydrology and Earth System Sciences. 16, 1817–1831. DOI: https://doi.org/10.5194/hess-16-1817-2012

[12] Pablos, M., Martínez-Fernández, J., Piles, M., et al., 2016. Multi-temporal evaluation of soil moisture and land surface temperature dynamics using in situ and satellite observations. Remote Sensing. 8(7), 587.

[13] Hamzeh, S., Mehrabi, M., Alavipanah, S.K., et al., 2018. Investigating the relationship between shallow groundwater, soil moisture and land surface temperature using remotely sensed data. In Proceedings of the IGARSS 2018 — 2018 IEEE International Geoscience and Remote Sensing Symposium, Valencia, Spain, 22–27 July 2018; pp. 7789–7792. DOI: https://doi.org/10.1109/IGARSS.2018.8518165

[14] Malik, M.S., Shukla, J.P., Mishra, S., 2021. Effect of groundwater level on soil moisture, soil temperature and surface temperature. Journal of the Indian Society of Remote Sensing. 49(9), 2143–2161. DOI:

https://doi.org/10.1007/s12524-021-01379-6

[15] Rivas, R.E., Weinzettel, P.A., Arias, D., et al., 1996. Groundwater monitoring network in the Arroyo del Azul watershed. Plains Hydrology Institute, Final Report. Available from: https://digital.cic.gba.gob.ar/items/ea3020d2-f0d9-4c1f-aeea-e2c2a77792ab (cited 20 August 2025). (in Spanish)

[16] Hargreaves, G.H., Samani, Z.A., 1982. Estimating potential evapotranspiration. Journal of Irrigation and Drainage Engineering. 108, 223–230.

[17] Copernicus Climate Change Service (C3S), 2017. ERA5 Ag: Agrometeorological indicators from 1979 to present derived from reanalysis. Available from: https://cds.climate.copernicus.eu/cdsapp#!/dataset/sis-agrometeorological-indicators?tab=overview (cited 20 August 2025).

[18] Malakar, N.K., Hulley, G.C., Hook, S.J., et al., 2018. An operational land surface temperature product for Landsat thermal data: methodology and validation. IEEE Transactions on Geoscience and Remote Sensing. 56(10), 5717–5735. DOI: https://doi.org/10.1109/TGRS.2018.2824828

[19] Li, Z.L., Wu, H., Duan, S.B., et al., 2023. Satellite remote sensing of global land surface temperature: Definition, methods, products, and applications. Reviews of Geophysics. 61(1), e2022RG000777

[20] Niclòs, R., Perelló, M., Puchades, J., et al., 2023. Evaluating Landsat-9 TIRS-2 calibrations and land surface temperature retrievals against ground measurements using multi-instrument spatial and temporal sampling along transects. International Journal of Applied Earth Observation and Geoinformation. 125, 103576. DOI: https://doi.org/10.1016/j.jag.2023.103576

[21] Huete, A.R., Jackson, R.D., Post, D.F., 1985. Spectral response of a plant canopy with different soil backgrounds. Remote Sensing of Environment. 17, 37–53.

[22] Jackson, R.D., Huete, A.R., 1991. Interpreting vegetation indices. Journal of Preventive Veterinary Medicine. 11, 185–200.

[23] Holzman, M.E., Rivas, R., Piccolo, M.C., 2014. Estimating soil moisture and the relationship with crop yield using surface temperature and vegetation index. International Journal of Applied Earth Observation and Geoinformation. 28, 181–192.